Hindawi
Shock and Vibration
Volume 2023, Article ID 7110987, 18 pages
https://doi.org/10.1155/2023/7110987

Research Article

Performance Assessment of Hybrid Fibre-Reinforced Concrete (FRC) under Low-Speed Impact: Experimental Analysis and Optimized Mixture

Abbas Sadeghian,[1] **Taleb Moradi Shaghaghi**,[1] **Yaghoub Mohammadi**,[2] **and Hossein Taghipoor**[3]

[1]*Department of Civil Engineering, Tabriz Branch, Islamic Azad University, Tabriz, Iran*
[2]*Department of Civil Engineering, University of Mohaghegh Ardabili, Ardabil, Iran*
[3]*Department of Mechanical Engineering, Velayat University, P.O. Box 99111-31311, Iranshahr, Iran*

Correspondence should be addressed to Yaghoub Mohammadi; yaghoubm@uma.ac.ir

Received 5 December 2022; Revised 6 February 2023; Accepted 24 February 2023; Published 11 March 2023

Academic Editor: Azwan I. Azmi

Fibre-reinforced concrete (FRC) has gained tremendous attention in many disciplines due to its high initial strength, favorable mechanical properties, structural lightness, and energy-absorbing properties. In this research, Barchip fibres, Forta, and Basalt are utilized to reinforce concrete under penetration effect loading to examine the energy absorption and impact strength characteristics. To determine the parameters of the percentage of fibres on the impact resistance properties, the Box–Behnken method as a subset of the response surface method (RSM) was used. A diagram of RSM is adopted to determine the optimal percentage of fibres for higher initial strength and energy absorption. Results obtained using Design-Expert software revealed an initial strength of 886.127 N and an optimal energy absorption of 4.9865 J. In addition, the calculated R2 values and normal probability graphs showed a fairy accurate correlation between the results of the experimental and mathematical approaches. Finally, this study evaluated the fracture surface, adhesion of the fibres to the concrete, and degradation modes of the fibres to pave the way for optimal utilization of these hybrid FRCs.

1. Introduction

For engineers, impact and severe load resistance remains an important challenge in terms of ensuring road traffic safety as well as the safety of vulnerable and old infrastructure [1]. Additionally, impact loads pose a serious threat to our built environment. During a storm, falling trees, collisions between vehicles, objects thrown at structures, and vehicle collisions with bridge piers can all cause impact loads on structures [2]. In consequence, concrete guardrails and airport pavements must be designed to withstand the impact of aircraft [3]. A study was conducted on the response of hybrid FRC under quasi-static load testing and also the impact of the projectile. Compared to conventional fibres, hybrid fibres improved beam quasi-static punching resistance as regards the behavior of load displacement and energy absorption [4].

The use of fibres in concrete has gained popularity in recent years as they have been found to improve the hardness and early strength of concrete. The majority of research has focused on testing reinforced concrete beams and slabs externally reinforced with FRP laminates in shear and flexure [5]. Engineered geopolymer composites (EGCs) with good thermal and mechanical properties were developed by Sindu and Sasmal [6]. Using impact loads, a fibre-reinforced geopolymer concrete beam was tested for its shear capacity. As a result of this study, it is suggested that when calculating the amount of energy imparted to the beam by the drop hammer, the variability in its kinetic energy should be considered [7]. These properties include abrasion

and impact resistance, decreased plastic shrinkage, settlement cracking, and contraction of permeability [8]. Researchers examined the effects of alkali-resistant glass fibres on manufactured aggregate properties through cold-bonding pelletization and the effect of processed aggregates on lightweight concrete production. Producing lightweight concrete with manufactured aggregates is both economical and environmentally advantageous [9]. Chemically, polymer fibres are synthetic fibres. Fibres made from polymers are commonly derived from petrochemical sources, including polyethylene, polyolefins, polyvinyl chloride, and phenol-formaldehyde [10]. The distinctly low cost of polypropylene fibres and their exact ductility properties make them one of the most popular types of synthetic fibres [11]. There are two types of polymer fibres: macrofibres and microfibres. The diameter of microfibres is less than 100 mm, and their length ranges between 5 and 30 mm. It has been proposed to use macropolymer fibres (MPFs) in shotcrete in place of steel fibres due to their enhanced energy absorption characteristics [12]. Research on PFRC has been extensive, but attempts have not been entirely successful in developing a model to predict tensile, compressive, and energy absorption behavior [13].

Randomly oriented fibres can enhance brittle behavior in concrete components, including concrete floors, as well as transfer of load, resistance to compression, strength in tensile, and flexibility. As a result of these improvements, the structural performance of foam concrete can be improved [14]. Researchers evaluated the effects of 3.3% volume fraction of polyvinyl alcohol fibres on 1000 kg/m^3 density foam concrete. Comparing the reinforced concrete foamed to the unreinforced concrete foamed, they found that reinforcement increased compressive and tensile strengths by 84.7% and 558%, respectively [15]. Metal fibres are the most common type of fibre used to enhance concrete [16], and fibres are made of synthetic materials [17]. In the case of foamed concrete, a viscosity-enhancing agent was used to increase the cohesion and consistency of the cement paste in its fresh state [18]. In accordance with Wu et al.'s evaluation of fibre-reinforced concrete's dynamic mechanical properties, concrete reinforced by fibres with a volume content of 0.2% is much better at improving concrete's mechanical properties than two other types of fibre concrete [17]. Researchers investigated how rubber concrete fractures under cyclic loading and found that concrete strength and elastic modulus decrease with increasing rubber content, while fracture energy increases [19]. The composite developed by Ranade et al. consists of 16 MPa, 5%, and 20% of high tensile strength, high ductility, and high energy dissipation capacity, respectively. [20]. RPUFs made from nonrenewable resources and nanostructured with BNC were studied by Chiacchiarelli et al. [21]. Combining flax fibres with basalt fibres produces better bending strength and flexural strength, while SEM analysis was used to study the failure morphology. In composites reinforced with flax fibre, impact bending is increased [22]. Natural fibres are becoming increasingly popular as reinforcement materials. There is an increasing demand for materials reinforced with natural fibres because it is possible to obtain materials that have superior mechanical properties, low density, and low cost. Furthermore, natural fibres are biodegradable, renewable, and environmentally friendly [23].

Forta-Ferro fibre is color-blended, easy to finish, and has a wide range of applications, produced from 100% virgin copolymer/polypropylene fibres with twisted monofilaments, providing a high-performance reinforcement system for concrete. A Forta-Ferro system reduces the shrinkage of plastics and hardened concrete, in addition to increasing impact energy, it also increases fatigue resistance and concrete toughness. Using a specific synergistic fibre system of long lengths, the ultra-heavy-duty fibre can provide maximum durability over time, structural improvements, and crack management during secondary/temperature cracks [24]. During their research, H-Nattaj and Nematzadeh studied the impacts of steel and Forta-Ferro fibres on high-strength concrete and also investigated the effects of silica fumes and nano-silica on fibre-reinforced concrete. According to this study, Forta-Ferro fibres enhanced concrete compressive strength by 16.9% according to volume fractions of 0.35 percent [25]. The shrinkage performance and mechanical properties of foamed concrete were improved when sisal fibre was added at 0.75%, according to Liu et al. [26]. They compared the properties of concrete without fibres, concrete with fibres, and Forta fibres of different types. Furthermore, they compared the advantages of Forta fibre over steel fibres. The researchers concluded that concrete without fibre is fragile, while concrete reinforced with Forta fibre prevents cracks from propagating [27].

How bar chip fibre length can influence early-age behavior and cracking resistance is investigated by Alnahhal and Aljidda [28] by applying concrete enriched with super absorbent polymers. Barchip fibres and internal curing materials can be used to improve the youthful properties of concrete [29]. Additionally, they found that increasing the percentage of Barchip fibre decreased the cracking potential of HSC. With an increase in Barchip fibre content from 0% to 0.3%, 0.6%, and 0.9%, the cracking potential parameter at 10.58 day decreased by 15.2%, 31.9%, and 44.3%, respectively [30]. As part of their study, Alwesabi and colleagues evaluated the strength of a composite made of steel, rubber, and polypropylene against impact. It can be concluded that hybridizing two fibres of steel and propylene boosts both the mechanical properties and strength of concrete simultaneously [31]. As a result of its excellent mechanical virtues and environmentally friendly manufacturing process, chopped basalt fibre is increasingly used for reinforcing concrete [32–34]. Performance improvement of adding basalt fibres to concrete is studied via drop-weight impact tests on concrete specimens cast with three different fibre mixtures. By adding BF to concrete, flexural strength was increased, but impact strength was not increased [35]. According to Adesina, pulverized composites of basalt reinforced cement exhibit improved mechanical properties and durability and demonstrate an enhancement in the mechanical characteristics of cement-like composites [36].

Research conducted examined the impact resistance and fracture properties of self-compacting concrete reinforced

with basalt, glass, and polypropylene fibre. A combination of basalt fibre, glass fibre, and polypropylene fibre increased flexural strength, impact resistance, and fracture energy but not compressive strength [37–39]. Recently, single fibre reinforced concrete was studied under weight loss tests. In comparison with ordinary concrete, Forta fibres significantly improved energy absorption and initial strength due to the high deformation of plastic and the occurrence of bridging phenomena [40].

The main motivation of this study is threefold: (i) to investigate the energy absorption and impact strength of FRC consists of Basalt, Barchip, and Forta hybrid fibres under low-speed impact loading; (ii) to calculate the fibres' effects on energy absorption and initial strength by modeling the interaction rate between the fibres; and (iii) to propose the optimized fibre percentage of the studied hybrid FRC subjected to impact load. In this regard, the importance of this paper is highlighted due to the lack of well-documented studies and the key role of hybrid FRCs in the design and construction of civil structures. The results are also statistically reviewed and analyzed, and finally, the optimal fibre content is determined for maximum strength and energy absorption.

2. Details of the Experiment

2.1. The Materials. In this study, gravel and sand from Ardabil were used as aggregates for concrete specimens. From the Namin region of Ardabil, fine-grained materials, including natural type sand that have been washed twice and gravel, as a coarse-grained broken type material were prepared. The sand and natural gravel are finely sieved through 3.8 sieves, respectively, to create a homogeneous concrete, while the remainder is sieved through grade 8 sieves. Table 1 and Figures 1(a) and 1(b) show a continuous grain size distribution, Table 1 and Figures 1(a) and 1(b) show a continuous grain size distribution. Table 1 shows aggregates' properties (i.e., the percentage of passing sands and gravels from fine to coarse sieve sizes) in concrete. Furthermore, Figure 1 shows the cumulative passing of the sands and gravels used in this study, and their position according to the upper- and lower-bound limits proposed by the ASTM-C33 standard. As can be seen, the gravel and sand sizes are within the permitted range according to this regulation. We used 3130.5 kg/m^3 Portland pozzolanic cement manufactured by the Ardabil Cement Factory in this study. The used fibres are Forta fibres from the FORTA company, Barchip fibres from the EPC company (elastic-plastic concrete), and Basalt fibres from Basalt fibres company. Figure 2 graphically represents the length of the studied fibres to reinforce the concrete, while the mechanical properties of are tabulated in Table 2.

2.2. The Fabrication of Fibre-Reinforced Concrete. The concrete combination was prepared during the specimen fabrication stage, which is identical for all specimens. Weights of materials according to the mixing plan ACI-211 are tabulated in Table 3, while Table 4 introduces the concrete-to-gravel-to-sand and water-to-cement ratios. The range of changes in the percentage of fibres in reinforced concrete under impact testing has been selected according to the manufacturer's report and the experiences of past studies. Three different changes have been selected for Basalt fibres, Forta fibres, and Barchip fibres. The figures for Basalt fibres are {0.25, 0.5, 0.75}, for Forta fibres {0.1, 0.3, 0.5}, and for Barchip fibres {0.15, 0.3, 0.45}. In the next step, for each specimen separately, according to the percentage of the fibres shown in Table 5 and Figure 3, all fibres are mixed together. After that, we mixed concrete and fibres for five minutes with a hand mixer at room temperature. This will create a perfectly homogeneous concrete mixture.

Lastly, each compound is poured into its mold and shaken for 10 minutes according to Figure 4. According to the Iranian concrete regulations, the concrete specimens are being fabricated in the laboratory for 24 hours and then cured in water for 28 days. Next, fifteen specimens measured 100 mm by 100 mm by 10 mm were prepared. Figure 5 shows the concrete combination after continuity and its granulation structure.

According to the design of experiments, 15 test modes with three central points are determined as a test of repeatability and a test error percentage. In Table 5, formulations of samples according to the Box–Behnken experimental design are also shown. The specimens under impact loading are named using three letters in Table 5. There are three types of fibres in concrete: basalt fibres, Forta fibres, and Barchip fibres. In our tests, for example, B.F.C-0.25-0.1-0.3 refers to 0.25% Basalt, 0.1% Forta, and 0.3% Barchip fibres, respectively. The drop hummer impact tester is used to test hybrid FRC specimens experimentally to provide the energy required for applying penetration impacts by means of a 2 kg weight free fall from 1 m above. Figure 6 represents our real testing machine, which consists of a magnet, an accelerometer, a load cell, and a specimen.

2.3. Parameters in Impact Resistance Behavior. Now, the attention is turned to study the absorbed energy of RC specimens and analyze their performance and impact strength [1, 2]. Impact strength is the amount of force that occurs at the onset of fracture and destruction of concrete under an impact load. After this point, the load drops dramatically, and the concrete loses its strength due to penetration and total destruction. The fluctuation of the load in this region determines the energy absorption by the energy absorber. The ideal state in the penetration process is to keep the force constant, which requires a constant strength and high strength of the fibres used in concrete due to the penetration of the impact during the progress process. The absorbed energy capacity can be calculated using the integration of the penetration force relative to the displacement. Obviously, through mechanical relations, this value is simply obtained from the area under the force-displacement diagram and the following equation (1).

$$E_a = \int_0^{\delta_{\max}} F(\delta)\mathrm{d}\delta\,(\mathrm{J}), \tag{1}$$

Table 1: The aggregates' properties.

Sieve size (mm)	Sand aggregate (% passing)	Gravel aggregate (% passing)
12.5	100	100
9.5	100	65.68
4.75	97.2	12.58
2.36	91.5	1.08
1.18	64	0.98
0.3	9	0.85

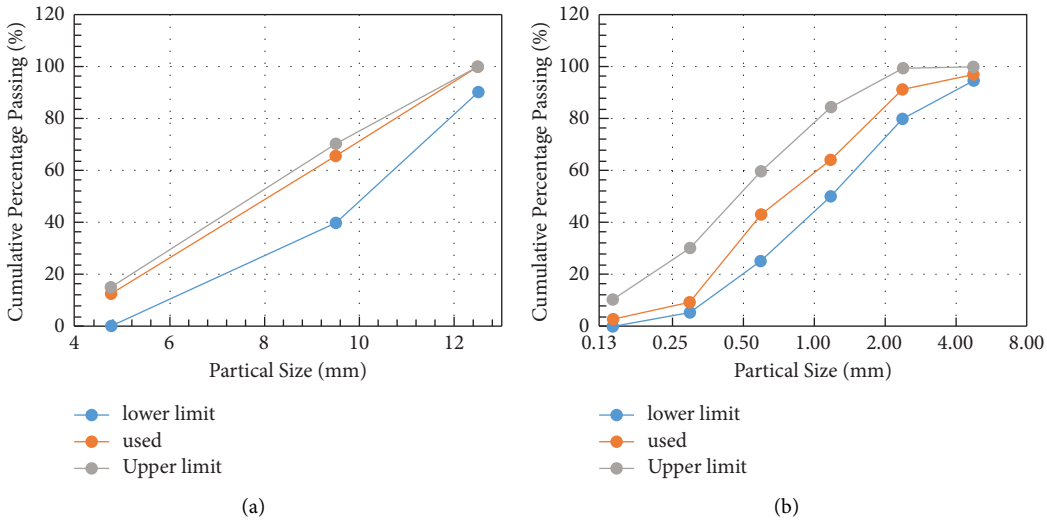

Figure 1: Particle size distributions: (a) gravel and (b) sand aggregate.

Figure 2: Length of fibres: (a) Basalt. (b) Forta. (c) Barchip.

Table 2: Mechanical properties of fibres.

Type of fibres	Density (g/cm^3)	Tensile strength (MPa)	Young's modulus (GPa)	Matrix adhesion	Acid/alkali resistance
Basalt fibres	2.67	4839	89	Good	Excellent
Forta fibres	0.91	640	12	Good	Excellent
Barchip fibres	0.91	660	6.4	Good	Excellent

Table 3: Weights of materials according to mixing plan ACI-211.

Gravel aggregate (kg/m^3)	Sand aggregate (kg/m^3)	Cement (kg/m^3)	Water (kg/m^3)	Water/cement ratio
1020	788	480	216	0.45

Table 4: Concrete by proportion.

Proportion by weight C : G. A : S. A	Water/cement ratio by weight
1 : 2.13 : 1.64	0.45

C: cement; G. A: gravel aggregate; S. A: sand aggregate.

where E_a is the absorbed energy in terms of the maximum penetration of the projectile in concrete (δ_{max}) and F is the penetration force during the projectile penetration process in concrete.

3. Numerical and Experimental Analysis

3.1. Variance Analysis. Finding the most contributing factors is of prime importance, and this can be achieved by applying different sensitivity analysis techniques [41]. In this study, analysis of variance (ANOVA) has been utilized to investigate the role of the percentage of fibres in both the initial strength and energy absorption, as our two performance assessment metrics.

ANOVA gives information about the contribution of each geometric parameter and its error. Affecting parameters are assumed to have a P value less than 0.05. In this context, components of the second-order model that do meet the defined statistical significance condition (i.e., $P < 0.05$) from the final equation of the studied two performance metrics are excluded. In this paper, the results of the ANOVA technique for impact strength and absorption energy competency are tabulated in Tables 6 and 7, respectively. As can be seen, the coefficient of determination (R^2) and the adjusted coefficient of determination (adj-R^2) are introduced in these tables to demonstrate the accuracy of predictions.

In accordance with the force-displacement diagram shown in Figure 7, three identical specimens were tested to verify the accuracy of the test. The results show that the maximum difference in the initial strength force between the three specimens is equal to 10%, and the minimum difference is 3.5%. Also, comparing the results of energy absorption between the specimens, it was found that there is a maximum difference of 11% and a minimum of 4.5% between the results, which is acceptable due to the nature of the load. Also, in the analysis of variance Tables 6 and 7, considering the studied performance metrics (i.e., initial strength and energy absorption criteria), the calculated errors are acceptable for engineering practices.

3.2. The Impact Strength Response. For the impact strength response, the results of the second-order model show the percentage of Basalt, Forta, and Barchip, as well as Forta and Barchip fibres by a double interaction between the three parameters. The transfer function is shifted to 0.45 to boost the accuracy of prediction models, leading to values of R^2 and R^2_{adj} to be close to each other as a result of better convergence to 1.0 (as the best prediction output). It should also be noted that a high value of R^2 indicates the independent effect of each parameter in the model, which determines the changes in the responses. In addition, the value of R^2_{adj} shows the real impact of the model parameters on the responses, which is high and close to the 1.0 value, reflecting a good prediction of the output model. The values of R^2 and R^2_{adj} were 0.9879 and 0.9757, respectively. Accordingly, the capability of the predictive initial strength models is demonstrated in an accurate way. Finally, equation (2) proposes the formula for the initial strength response:

$$\begin{aligned}(\text{Peak force})^{0.45} = {} & +18.54061 + 13.01406 \times \text{Basalt} - 5.26807 \times \text{Forta} \\ & -41.75286 \times \text{Barchip} + 27.92069 \times \text{Basalt} \times \text{Forta} \\ & +114.92581 \times \text{Forta} \times \text{Barchip} - 14.72121 \times \text{Basalt}^2 \\ & -48.46427 \times \text{Forta}^2.\end{aligned} \tag{2}$$

The peak force response can be estimated via equation (2) based on the actual factors for specific levels of each factor. For each factor, we suggest specifying the levels in terms of original units. Given that the coefficients of this equation are scaled to consider the units of each factor, and the intercept is not located in the middle of the design space, it is not recommended to find to determine each factor's relative effect.

The bar chart in Figure 8 shows the initial strength or strength of hybrid concrete specimens. The B.F.C-0.5-0.5-0.45 specimen had the highest strength. The B.F.C-0.75-0.3-0.15 and BFC-0.75-0.5-0.3 specimens are in second place with the initial strength close to each other, having a 13.3% decrease in strength compared to the B.F.C-0.5-0.5-0.45 specimen. The lowest decrease in initial strength is related to the B.F.C-0.5-0.1-0.45 specimen, which decreased by 750% compared to the B.F.C-0.5-0.5-0.45 specimen.

3.3. The Energy Absorption Response. Similar to Section 3.2, we seek to propose a regression formula for the adsorption force output unitizing a second-order model considering a dual interaction between Basalt fibre percentage, Forta fibre percentage, and Barchip fibre percentage. The values of R^2 and R^2_{adj} were calculated 0.9818 and 0.9676, respectively, proving the accuracy of the prediction model. Similarly, considering the P-value threshold equal to 0.05, where the second-order term for the Forta fibre percentage parameter and the double interaction between Basalt and Forta fibre percentage, "Basalt × Forta," and the fibres of Forta and

Table 5: Fibre percentage and impact test results at low speed.

Samples	Basalt (%)	Forta (%)	Barchip (%)	Energy absorption (J)	Impact strength (N)
B.F.C-0.25-0.1-0.3	0.25	0.1	0.3	1.11112	254.026
B.F.C-0.75-0.1-0.3	0.75	0.1	0.3	1.0672	241.325
B.F.C-0.25-0.5-0.3	0.25	0.5	0.3	1.7627	381.039
B.F.C-0.75-0.5-0.3	0.75	0.5	0.3	4.32336	762.079
B.F.C-0.25-0.3-0.15	0.25	0.3	0.15	2.56676	444.959
B.F.C-0.75-0.3-0.15	0.75	0.3	0.15	4.43198	763.179
B.F.C-0.25-0.3-0.45	0.25	0.3	0.45	1.92035	317.533
B.F.C-0.75-0.3-0.45	0.75	0.3	0.45	3.90554	571.559
B.F.C-0.5-0.1-0.15	0.5	0.1	0.15	1.53148	539.806
B.F.C-0.5-0.5-0.15	0.5	0.5	0.15	2.14723	482.65
B.F.C-0.5-0.1-0.45	0.5	0.1	0.45	0.592491	101.611
B.F.C-0.5-0.5-0.45	0.5	0.5	0.45	4.35683	863.689
B.F.C-0.5-0.3-0.3	0.5	0.3	0.3	2.80879	596.962
B.F.C-0.5-0.3-0.3	0.5	0.3	0.3	2.52964	576.983
B.F.C-0.5-0.3-0.3	0.5	0.3	0.3	2.68373	540.994
B.F.C-0-0-0	0	0	0	0.7479	177.818
BFC-0.64-0.44-0.41 (opt1)	0.649	0.445	0.415	4.678	786.5437
BFC-0.73-0.47-0.37 (opt2)	0.735	0.473	0.37	4.599	838.68

Figure 3: Combination of three fibres of Basalt, Barchip, and Forta.

Figure 4: Make molds and specimens separately.

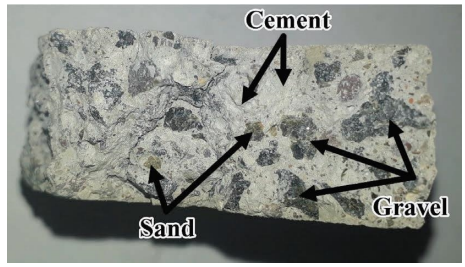

Figure 5: Structural composition and granulation of concrete after cohesion.

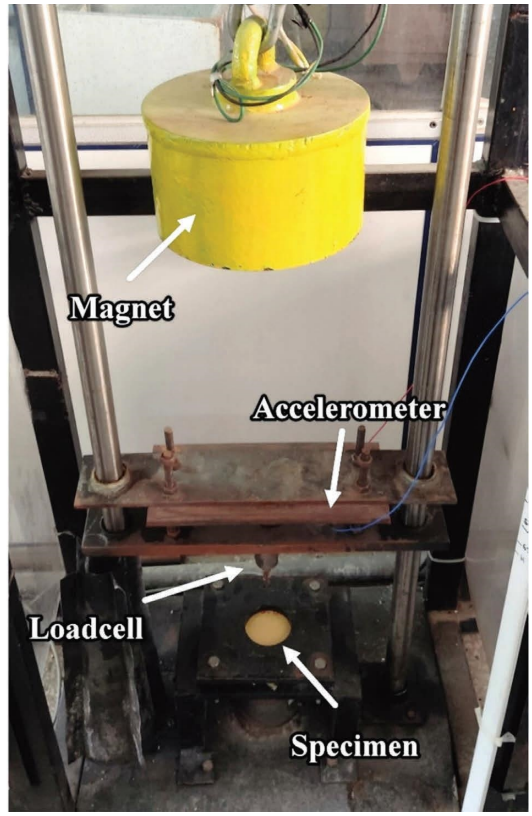

Figure 6: The setting of the utilized drop hummer test device for impact tests in this study.

Barchip, "Forta × Barchip" are modeled. Furthermore, the response has been powered by −0.07 to refine the accuracy. The final energy absorption relationship is proposed as equation (3):

$$\begin{aligned}(\text{Energy absorption})^{-0.07} = {} & +0.952080 + 0.023401 \times \text{Basalt} - 0.264465 \times \text{Forta} \\ & +0.321407 \times \text{Barchip} - 0.306550 \times \text{Basalt} \times \text{Forta} \\ & -0.937672 \times \text{Forta} \times \text{Barchip} + 0.870985 \times \text{Forta}^2.\end{aligned} \tag{3}$$

The bar chart in Figure 9 shows the energy absorbed by hybrid concrete. The results show that the specimen B.F.C-0.75-0.3-0.15 had the highest energy absorption the results of the diagram show that the specimens with the highest Basalt fibres have the highest energy absorption. B.F.C-0.5-0.5-0.45 and B.F.C-0.75-0.5-0.3 specimens are in the second place with very little difference in the highest energy absorption, which has decreased by 2.48 and 1.72 compared to B.F.C-0.75-0.3-0.15, respectively. The B.F.C-0.5-0.1-0.45 specimen had the lowest energy absorption, which decreased by 648% compared to the specimen with the highest energy absorption.

Table 6: Impact strength analysis of variance (ANOVA) table.

Source	Sum of squares	d*f*	Mean square	*F*-value	*P* value	
Model	166.89	7	23.84	81.34	<0.0001	Significant
A. Basalt	22.24	1	22.24	75.87	<0.0001	
B. Forta	63.54	1	63.54	216.78	<0.0001	
C. Barchip	9.53	1	9.53	32.50	0.0007	
AB	7.80	1	7.80	26.60	0.0013	
BC	47.55	1	47.55	162.21	<0.0001	
A^2	3.14	1	3.14	10.73	0.0136	
B^2	13.96	1	13.96	47.62	0.0002	
Residual	2.05	7	0.2931			
Lack of fit	1.75	5	0.3495	2.29	0.3308	Not significant
Pure error	0.3046	2	0.1523			
Cor total	168.94	14				
			Std. dev	0.5414	R^2	0.9879
			Mean	15.91	Adjusted R^2	0.9757
			C.V. %	3.40	Predicted R^2	0.9181
					Adeq precision	31.6957

Table 7: Analyses of variance (ANOVA) for the absorption of energy.

Source	Sum of squares	d*f*	Mean square	*F*-value	*P* value	
Model	0.0212	6	0.0035	70.61	<0.0001	Significant
A-Basalt	0.0024	1	0.0024	46.89	0.0001	
B-Forta	0.0100	1	0.0100	198.74	<0.0001	
C-Barchip	0.0003	1	0.0003	5.78	0.0430	
AB	0.0009	1	0.0009	18.75	0.0025	
BC	0.0032	1	0.0032	63.14	<0.0001	
B^2	0.0045	1	0.0045	90.39	<0.0001	
Residual	0.0004	8	0.0001			
Lack of fit	0.0004	6	0.0001	5.35	0.1659	Not significant
Pure error	0.0000	2	0.0000			
Cor total	0.0216	14				
			Std. dev	0.0071	R^2	0.9815
			Mean	0.9475	Adjusted R^2	0.9676
			C.V. %	0.7473	Predicted R^2	0.9169
					Adeq precision	28.3648

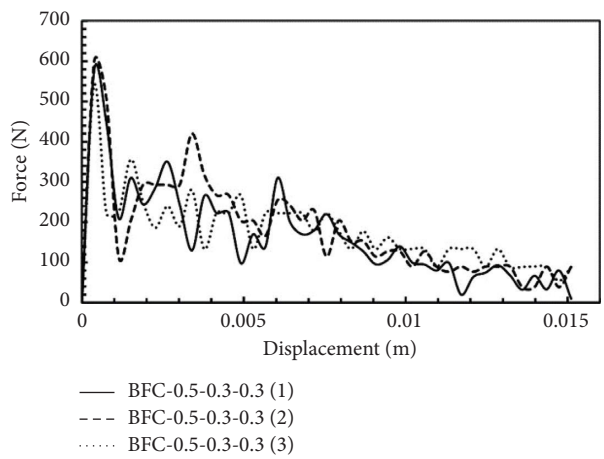

Figure 7: Force-displacement diagram for three identical specimens of BFC-0.5-0.3-0.3.

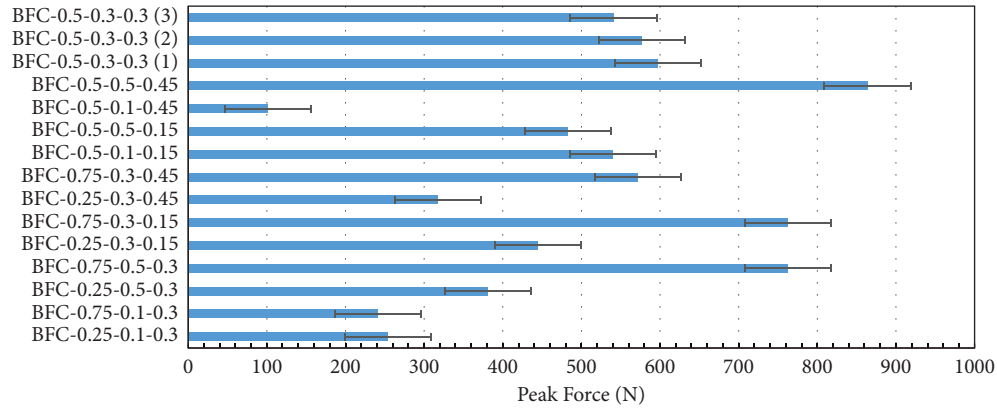

Figure 8: Bar chart of the strength of hybrid concrete specimens.

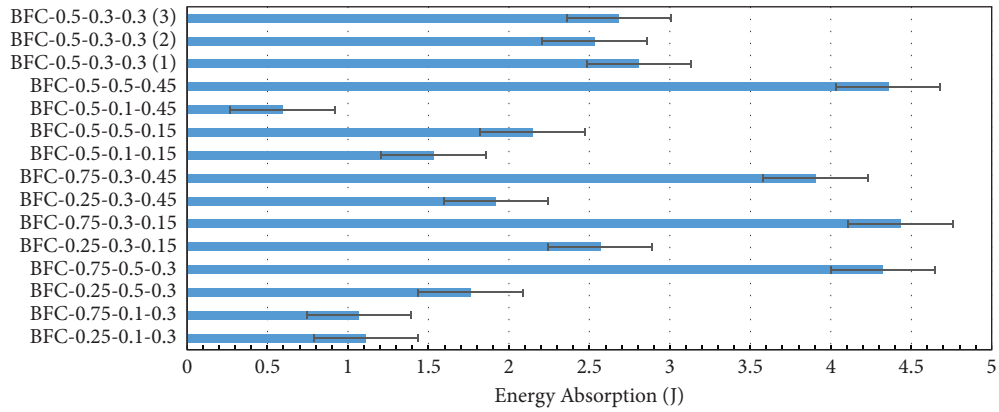

Figure 9: Bar chart of the energy absorption by hybrid concrete.

3.4. Statistical Validation. Probabilistic goodness-of-fit tests are of utmost importance to demonstrate the accuracy of prediction models. To this end, Figure 10 shows the normal plot of the residuals. As can be observed, the points are mostly situated in or in the close vicinity of the 45-degree red line, which demonstrates that a normal probability distribution is a proper candidate to be fitted to the data. Another approach to check the accuracy is the demonstration of residuals versus the predicted models, as shown in Figure 11. This diagram shows no regular structure among the design points, suggesting a constant variance. Analysis of variance assumptions are confirmed by these two forms. As the last statistical test, the YY-plots, demonstrating the predicted versus actual distribution, are depicted in Figure 12 by the final model obtained for the energy absorption and initial strength responses. As can be seen, both energy absorption behavior and impact strength metrics are calculated accuracy due to the points located near the diagonal line.

3.5. Quantifying the Effect of Fibre Weight Percent Parameters on Impact Strength and Energy Absorption. The sensitivity of weight percent of Basalt, Forta, and Barchip fibres to energy absorption and impact strength properties are shown in Figures 13(a) and 13(b), respectively. Changing the quantity of these three parameters independently can be summarized as follows: (i) increasing the weight percent of Barchip fibres in concrete drops both performance criteria and vice versa; (ii) basalt and Forta fibres act nonlinear in terms of peak force criterion; (iii) the nonlinear behavior of the Forta fibres in energy absorption behavior is more highlighted in the initial strength metric; (iv) rising the weight percent of Basalt fibres, increases energy absorption and initial strength and vice versa. The former metric follows a linear ascending trend, while the latter experiences a nonlinear pattern with a gentle slope; and (v) both performances witnessed a convex behavior when increasing the Forta fibres (a stronger one in energy absorption), whereas it decreases almost linearly by the reduction of mixture.

Figures 14 and 15 depict three-dimensional representations of the dual effect of the parameters simultaneously for the initial strength force and the absorbed energy, respectively. According to the Figure 14(a), it can be stated that at a high percentages of Barchip (45%), the variation range of initial strength with changes in the proportion of Forta fibres in concrete is greater than the low percentages. In other words, at low share of Barchip fibres (15%), the sensitivity of the impact strength to the weight percent of the Forta fibres

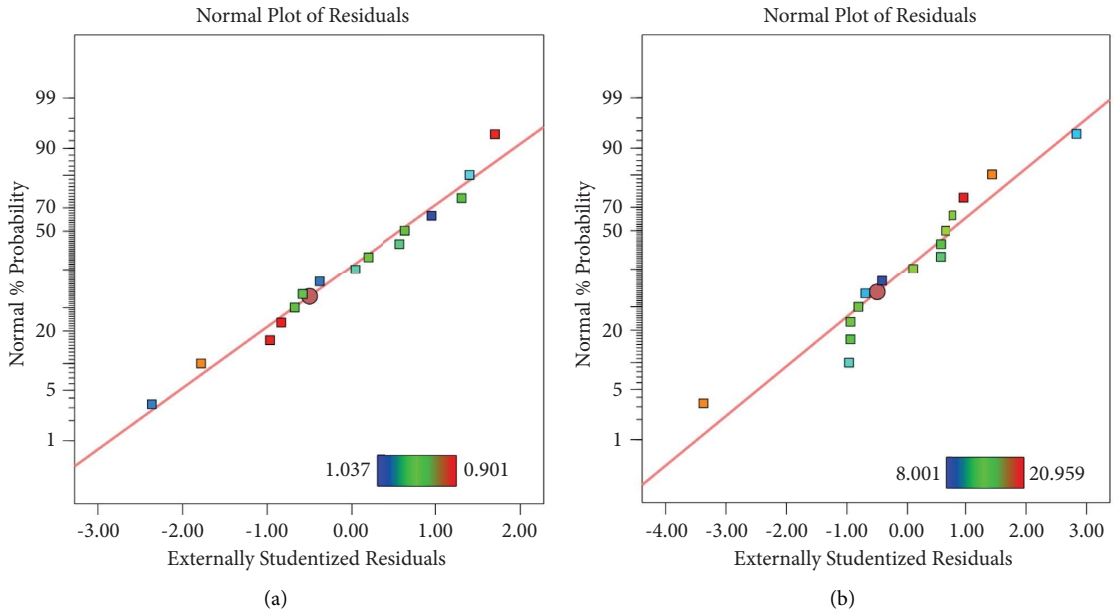

Figure 10: Normal probability of residuals: (a) energy absorption response and (b) impact strength response.

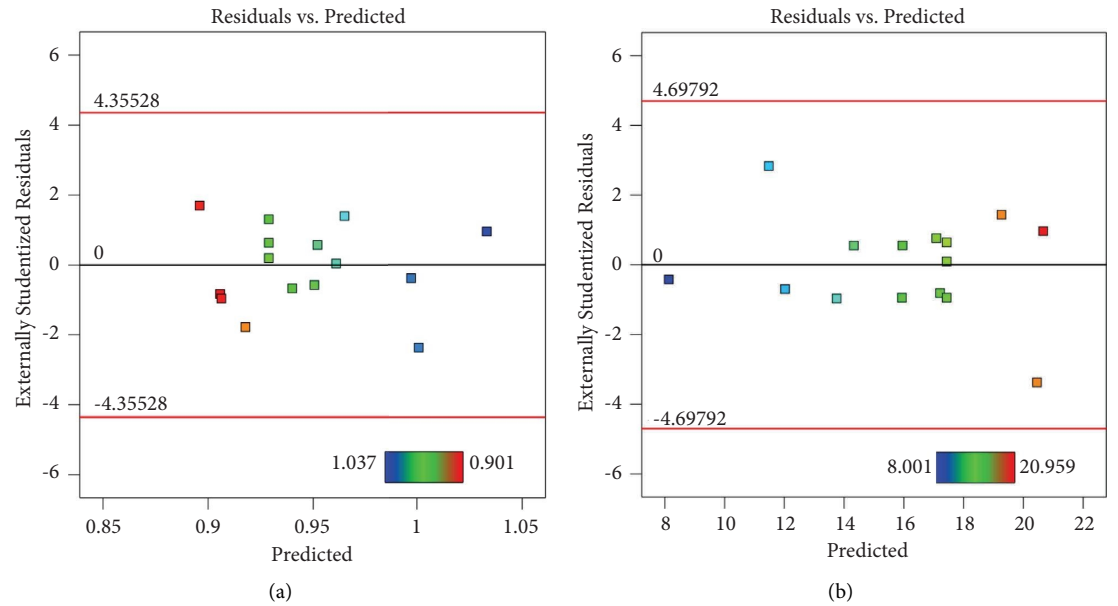

Figure 11: Diagrams of processed values to residuals: (a) energy absorption response and (b) impact strength response.

decreases. Figure 14(b) shows that the simultaneous interaction of the presence of Barchip and Basalt fibres in concrete for impact strength response is less than other binary fibre interactions. On the other hand, it can be seen in Figure 14(c) that the highest quantity of the impact strength is associated with the high weight percent of Basalt (75%) and Forta fibres (50%).

Figure 15(a) illustrates that the interaction between the weight percent of Forta and Barchip fibres for the absorbed energy is higher than other parameters in concrete. Therefore, at the high weight percent of Barchip fibres (45%) with the changes of Forta fibres, the variation range of the energy absorption increases sharply. This behavior is also seen in the dual interaction of the presence of Basalt and Forta fibres in concrete according to Figure 15(c). Figure 15(b) shows that the simultaneous interaction of the presence of Barchip and Basalt fibres in concrete for the energy absorption response is less than the other binary fibre interactions. In this figure, it can be seen that the maximum energy absorption occurs for the case where the weight percent of Basalt fibres is at maximum level and the weight percent of Barchip fibres has the lowest amount.

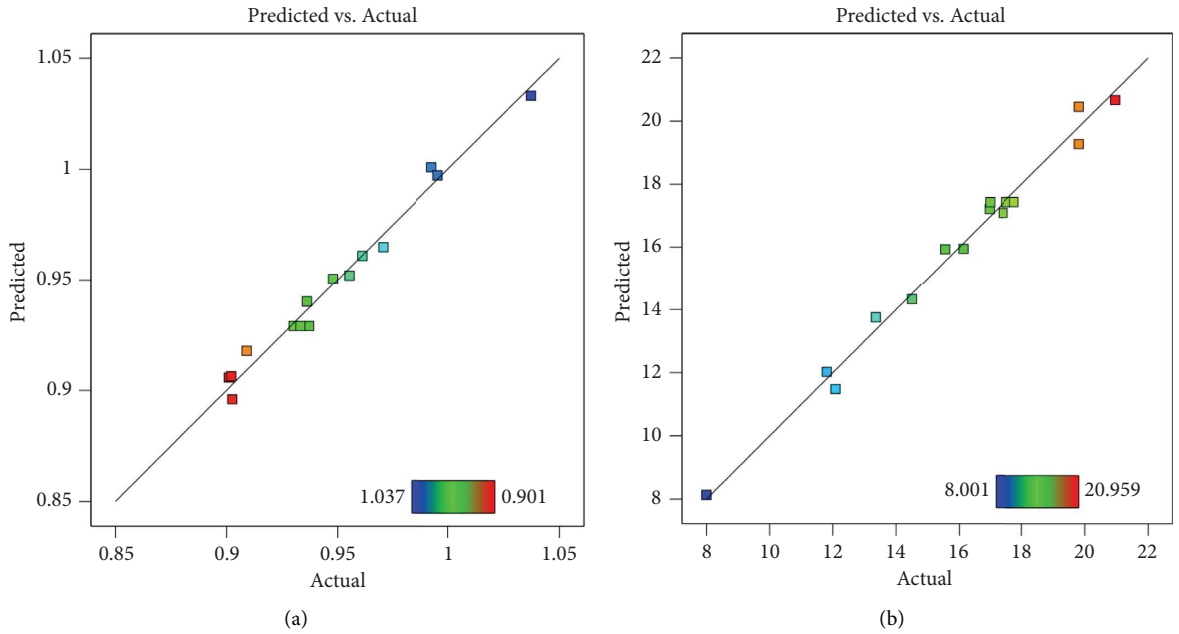

Figure 12: Diagrams of the fitted values to real values: (a) scatter of the energy absorption response and (b) scatter of the impact strength response.

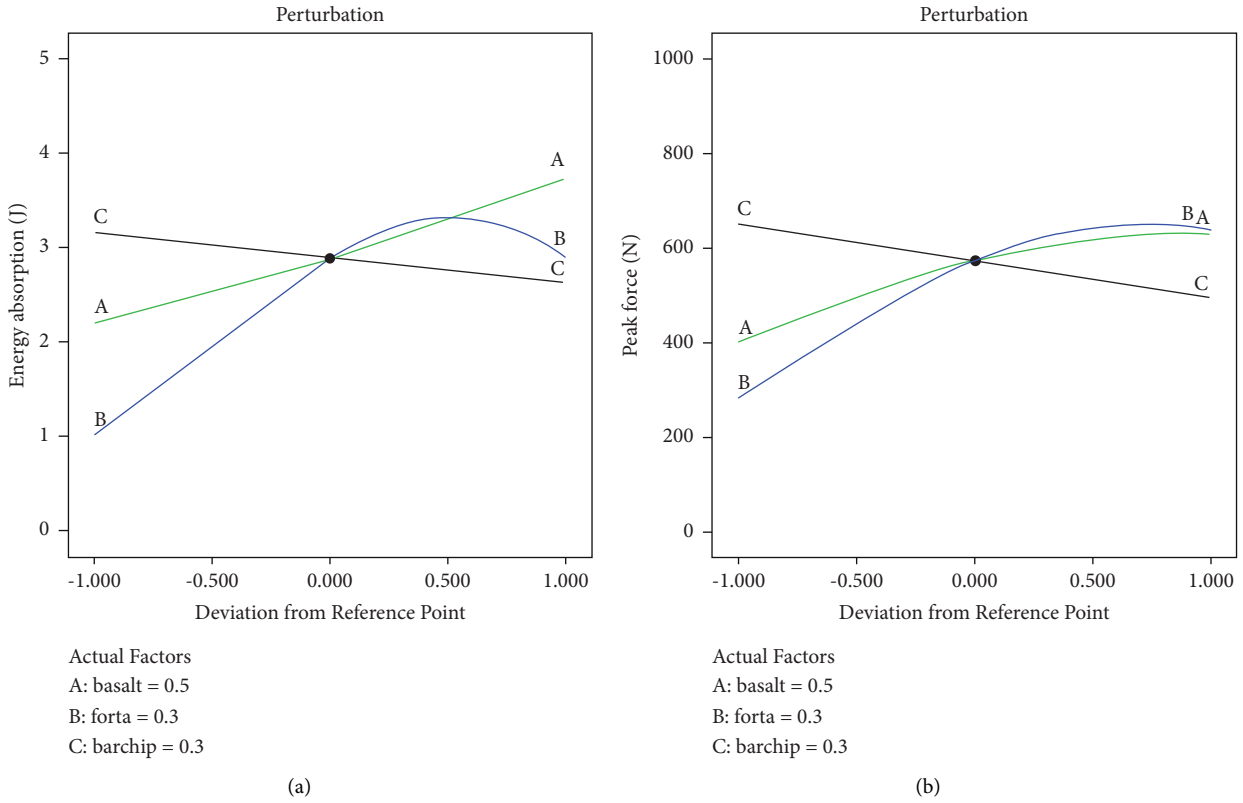

Figure 13: Diagram of sensitivity to changes in the fibre percentage parameters at (a) energy absorption and (b) impact strength.

3.6. Examination of the Fracture Surface. Figure 16 portrays the failure surfaces of reinforced concrete with Forta, Barchip, and Basalt fibres. In a comparative way, it can be seen that the cohesion between the fibres of Basalt and Forta with concrete is preferable. Only in the case of Barchip fibres, a pull-out phenomenon was resulted between the fibres and

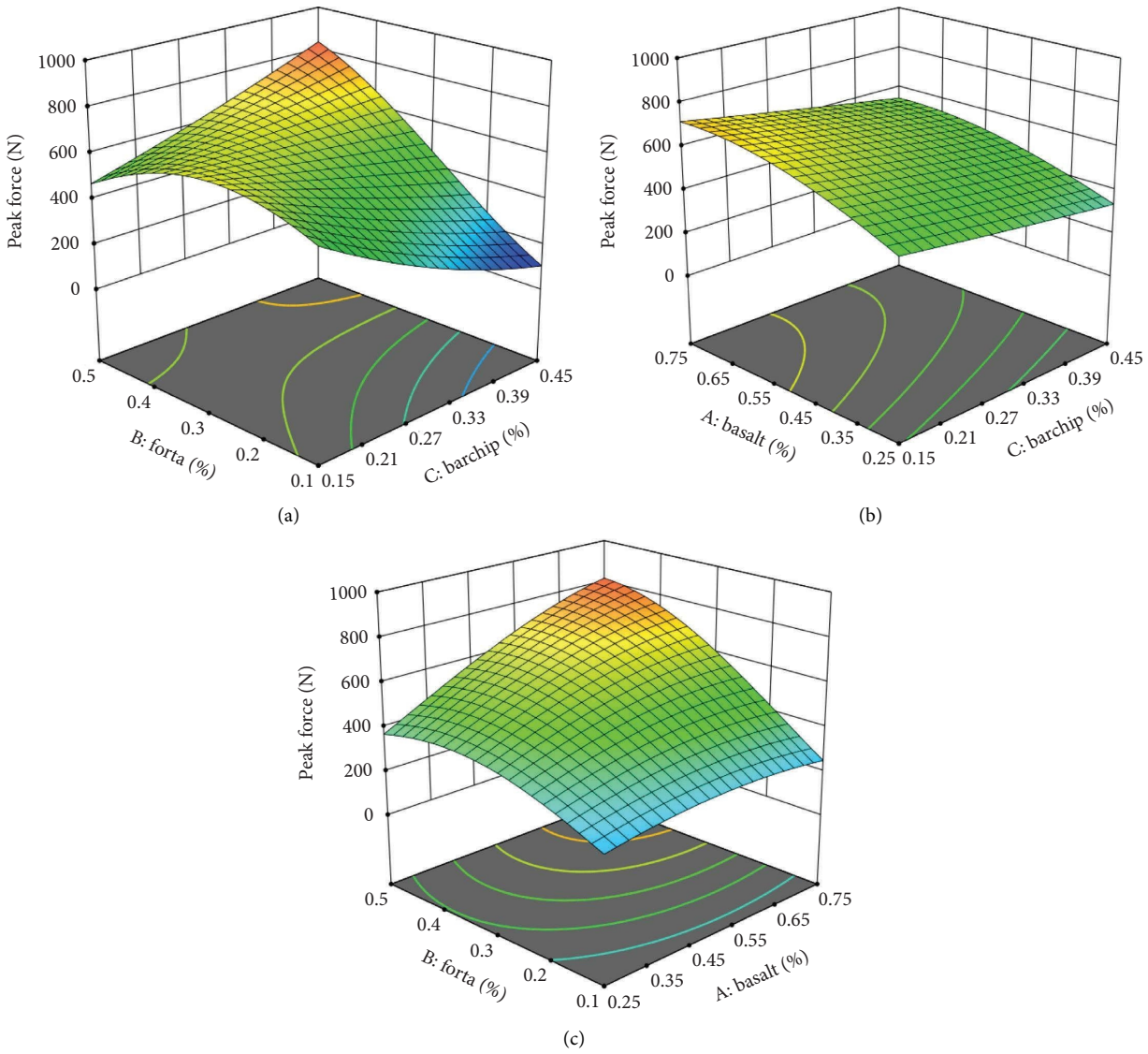

Figure 14: Three-dimensional diagram of the simultaneous effect of the parameters of (a) percentage of Forta and Barchip fibres, (b) percentage of Basalt and Barchip fibres, and (c) percentage of Forta and Basalt fibres on the impact strength.

the matrix concrete. Fibre breakage, cracking of the concrete underlying the hybrid fibre reinforcement, and global perforation are the chief mechanisms of energy absorption by the impactor in concrete structures reinforced by the hybrid fibres. Figure 17 shows the degraded concrete specimens after penetration impact testing. In Figure 18, the fibre specimen without the fibre reinforcement showed brittle fracture and low strength and energy absorption

The good adhesion of these fibres to the concrete also increases the stress required to break the fibres. Breaking of fibres is the most important mechanism of degradation for increasing concrete strength and energy absorption. Figure 19 shows the breakage of Basalt fibres. Considering the regular structure in conjunction with smaller dimensions of Basalt fibre reinforcement of concrete, it reduces stress at the points of connection between fibre and concrete, in comparison with Forta and Barchip fibres. According to the agglomeration and localized increases in stress concentration, excessive accumulation of the Basalt fibres in concrete significantly slumps the peak force.

Moreover, due to Forta fibre properties and numerous plastic deformations during the impact loading, the Forta fibres-reinforced concrete strengthens concrete's impact resistance behavior and increases its strength and absorption. As shown in Figure 19, fibre bridging in concrete by Forta fibres is the key feature to enhance the energy dissipation in specimens of concrete reinforced with fibres. Experimental results have demonstrated that the Forta fibres with a weight percent of 0.3 exhibit the highest energy dissipation and strength. Then, by increasing the weight percent of these fibres in concrete, the peak force decreases, which originates from high agglomeration of fibres in conjunction with the formation of dramatic local stress concentrations.

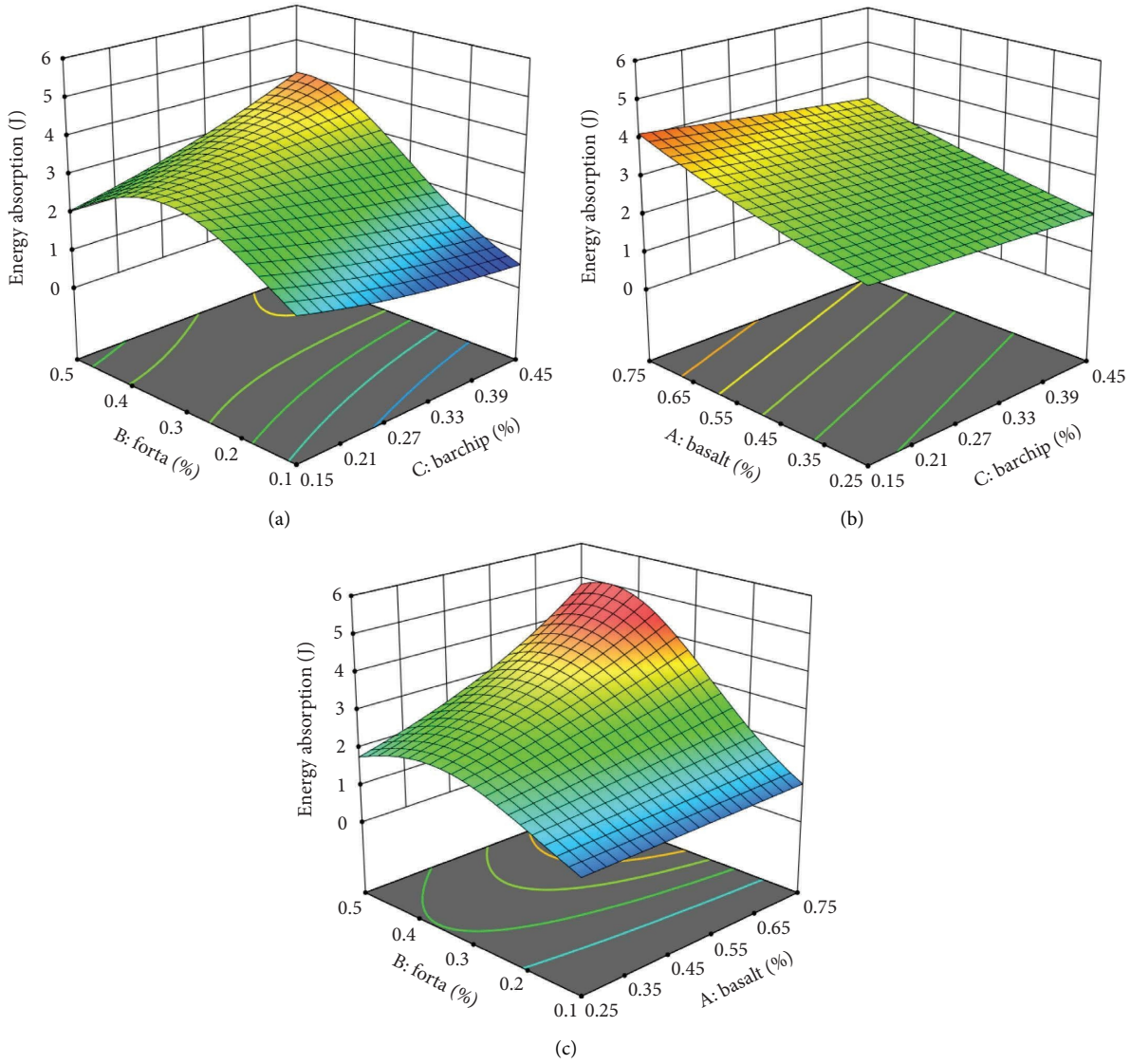

Figure 15: Three-dimensional diagram of the simultaneous effect of parameters of (a) percentage of Forta and Barchip fibres, (b) percentage of Basalt and Barchip fibres, and (c) percentage of Forta and Basalt fibres on energy absorption.

3.7. Optimization Results. According to the results obtained from analysis of variance and analysis performed on three parameters of weight percent of the Basalt, Forta, and Barchip fibres, optimization of energy absorption capacity and initial strength is done. Optimal values of the parameters that determine our design goals are determined. After studying the effect of the process parameters on the absorption capacity and strength of the hybrid FRC, the levels of these parameters that give the optimal point are determined. According to the BBD results, the optimal operating conditions for energy absorption are found to be the Forta fibre loading of 0.445 wt%, Basalt fibre loading of 0.649 wt%, and Barchip fibre loading of 0.415 wt%. Under these conditions, the predicted removal energy absorption is found to be 4.9865 J, as shown in Figure 20. The maximum value for initial strength is 886.127 N, and the utility function of the 100% has been determined that, the upper and the lower bounds of the parameters and responses are presented in Table 8. Also, the optimal distribution of the values of the parameters along with the maximum impact strength has been indicated in Figure 21. Under optimized conditions, experiments were conducted to verify the validity of the statistical and experimental strategies. The absorption and impact strength were presented as 4.678 J and 838.68 N, respectively. Results indicated that the difference between the experimental and optimization values was well within a 6% range, indicating the model's adequacy. Based on the excellent agreement between the optimization and experimental results, the validity of the model has been confirmed as well as the existence of the optimal solution. Figure 22 shows the force-displacement diagram for optimal specimens.

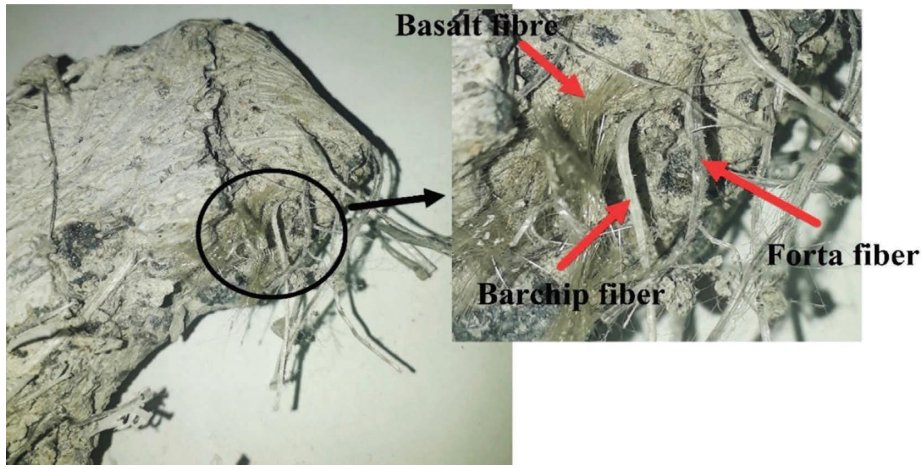

Figure 16: Fracture surface of the concrete specimen reinforced with the hybrid fibre (BFC-0.25-0.1-0.3).

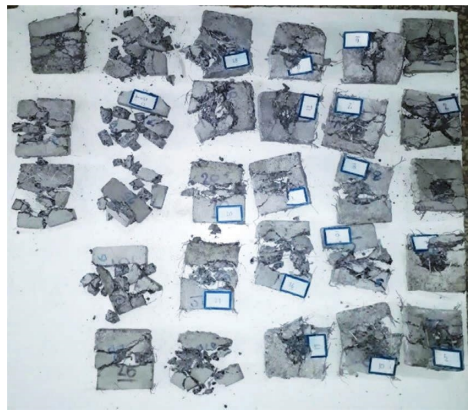

Figure 17: Test results after penetration impact.

Figure 18: Fibreless concrete specimen.

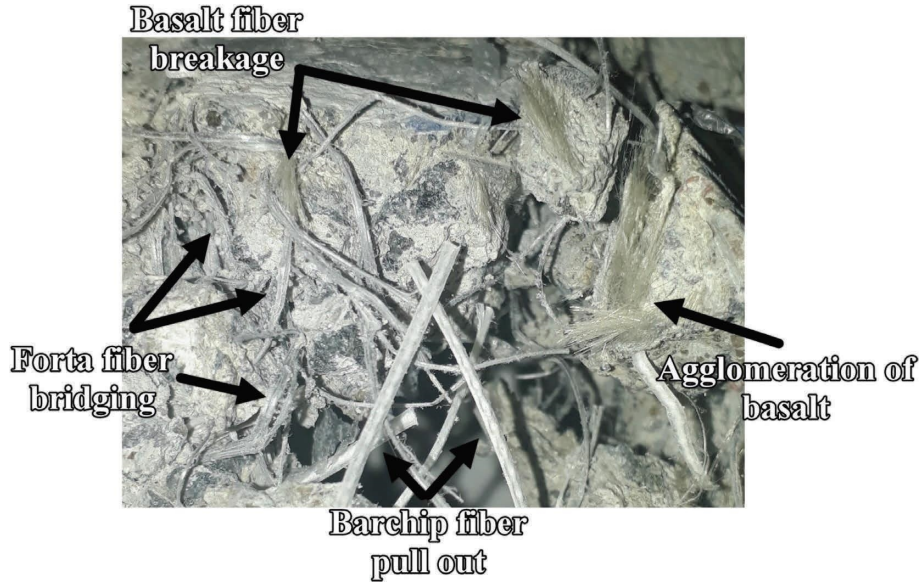

Figure 19: Fracture surface of the reinforced concrete (BFC-0.75-0.3-0.45).

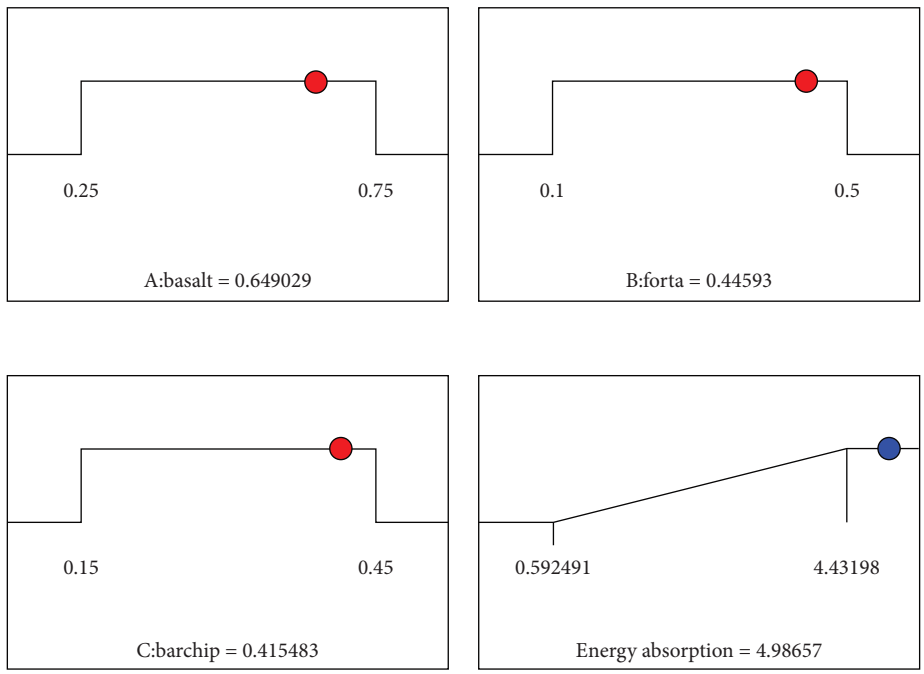

Figure 20: Optimal values of parameters and maximum energy absorption in the concrete panel under penetration impact.

Table 8: Values considered in optimizing the energy absorption-impact strength.

Significance	Weight	High limit	Lower limit	Target	unit	Indicator
3	1	0.75	0.25	In range	%	Basalt
3	1	0.5	0.1	In range	%	Forta
3	1	0.45	0.15	In range	%	Barchip
3	1	4.43195	0.59249	Maximize	J	Energy absorption
3	1	863.68963	101.611	Maximize	N	Impact strength

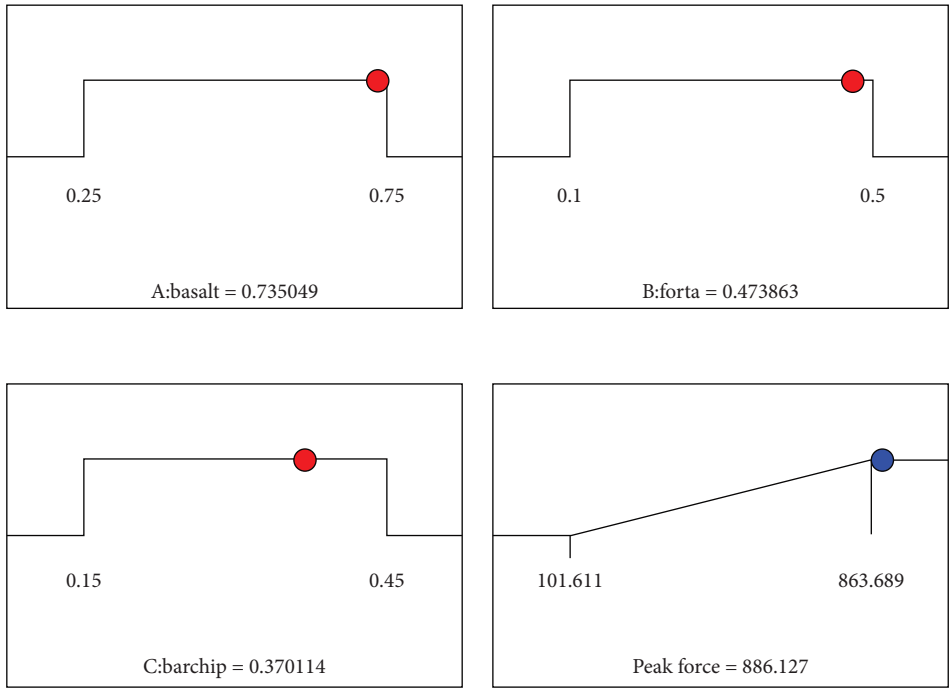

Figure 21: Optimal values of parameters and maximum impact strength in the concrete panel under penetration impact.

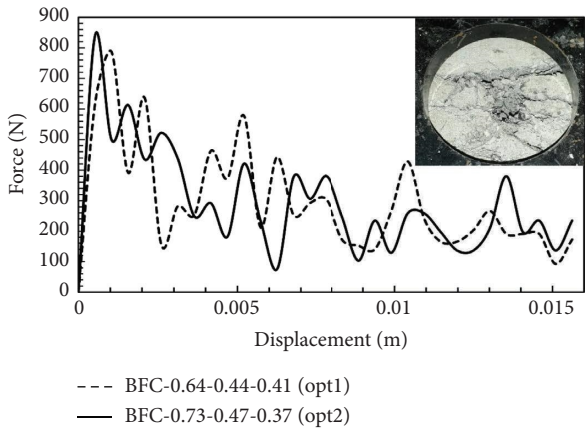

Figure 22: Force-displacement diagram for optimal specimens under impact loading.

4. The Conclusion

This study attempts to determine the efficacy of fibre addition on the slight-velocity impact behavior of fibre hybrid concrete by conducting fibre addition experiments. Hybrid concretes consisting of Basalt fibres with 0.25 to 0.75 wt%, Forta fibres with 0.1 to 0.5 wt%, and Barchip fibres with 0.15 to 0.45 wt% were made using the response surface method, which is one of the test design methods, and impacts were applied by using a spherical tip projectile. The descriptions of the results of this research are summarized as follows:

(i) In impact loading, there is not much adhesion between the Barchip fibres and concrete. Accordingly, no effective stress transfer between the concrete and the fibres is reported.

(ii) Fibres from Forta have been proven to increase the fracture toughness and fracture strength of hybrid concrete by bridging mechanisms between the concrete field and fibres.

(iii) Basalt fibres and concrete had negligible stress concentration between the connecting points and the interface. It is this stress that leads to fibre breakage.

(iv) The amount of basalt fibres in a material increases its energy absorption, but its strength decreases due to the phenomenon of agglomeration when the amount is high.

(v) According to the optimization results, the maximum energy absorption and initial strength are 4.9865 J and 886.127 N, respectively.

(vi) Application of uncertainty-aware optimization techniques [42] can pave the way for future studies using the developed experimental dataset by this study.

(vii) According to the BBD results, the optimal operating conditions for energy absorption are found to be the Forta fibre loading of 0.445 wt%, Basalt fibre loading of 0.649 wt%, and Barchip fibre loading of 0.415 wt%. Under these conditions, the predicted removal energy absorption is found to be 4.9865 J. In addition, the maximum value for initial strength is 886.127 N, and the utility function of the 100% has been determined. The optimized mixtures are within the upper and lower bounds of the parameters and responses.

(viii) Under optimized conditions, experiments were conducted to verify the validity of the statistical

and experimental tests. The absorption and impact strength were presented as 4.678 J and 838.68 N, respectively. Results indicated that the difference between the experimental and optimization values was well within a 6% range, indicating the model's adequacy. Based on the excellent agreement between the optimization and experimental results, the validity of the model has been confirmed as well as the existence of the optimal solution.

Data Availability

The experimental dataset, which is carried out for the first time by authors, is already introduced completely in the manuscript (see Table 4), while the optimization results can be found in other parts.

Ethical Approval

In this article, no studies have been conducted on humans or animals by the authors.

Conflicts of Interest

The authors declare that they do not have any conflicts of interest.

References

[1] C. Fallon and G. McShane, "Experimental and numerical investigation on the impact response of elastomer-coated concrete," *Multidisciplinary Digital Publishing Institute Proceedings*, vol. 2, no. 8, p. 387, 2018.

[2] R. Ranade, V. C. Li, W. F. Heard, and B. A. Williams, "Impact resistance of high strength-high ductility concrete," *Cement and Concrete Research*, vol. 98, pp. 24–35, 2017.

[3] L. Prochowski, "Analysis of displacement of a concrete barrier on impact of a vehicle. theoretical model and experimental validation," *Journal of kones*, vol. 17, no. 4, pp. 399–406, 2010.

[4] T. Almusallam, A. Abadel, N. Siddiqui, H. Abbas, and Y. Al-Salloum, "Impact behavior of hybrid-fibre reinforced concrete beams," *Structures*, vol. 39, pp. 782–792, 2022.

[5] I. Jankowiak, "Analysis of RC beams strengthened by CFRP strips—experimental and FEA study," *Archives of Civil and Mechanical Engineering*, vol. 12, no. 3, pp. 376–388, 2012.

[6] B. S. Sindu and S. Sasmal, "On the development and studies of nano- and micro-fiber hybridized strain hardened cementitious composite," *Archives of Civil and Mechanical Engineering*, vol. 19, no. 2, pp. 348–359, 2019.

[7] T. T. Tran, T. M. Pham, Z. Huang et al., "Effect of fibre reinforcements on shear capacity of geopolymer concrete beams subjected to impact load," *International Journal of Impact Engineering*, vol. 159, Article ID 104056, 2022.

[8] F. Bencardino, L. Rizzuti, G. Spadea, and R. N. Swamy, "Experimental evaluation of fiber reinforced concrete fracture properties," *Composites Part B: Engineering*, vol. 41, no. 1, pp. 17–24, 2010.

[9] K. S. Vali and S. B. Murugan, "Impact of manufactured fibre aggregate in the production of lightweight concrete," *Materials Today Proceedings*, vol. 65, no. 2, pp. 1690–1696, 2022.

[10] M. G. Alberti, A. Enfedaque, and J. C. Gálvez, "Fibre reinforced concrete with a combination of polyolefin and steel-hooked fibres," *Composite Structures*, vol. 171, pp. 317–325, 2017.

[11] F. Aslani and S. Nejadi, "Self-compacting concrete incorporating steel and polypropylene fibers: compressive and tensile strengths, moduli of elasticity and rupture, compressive stress–strain curve, and energy dissipated under compression," *Composites Part B: Engineering*, vol. 53, pp. 121–133, 2013.

[12] V. Jovičić, J. Šušteršič, and Ž. Vukelič, "The application of fibre reinforced shotcrete as primary support for a tunnel in flysch," *Tunnelling and Underground Space Technology*, vol. 24, no. 6, pp. 723–730, 2009.

[13] R. Babaie, M. Abolfazli, and A. Fahimifar, "Mechanical properties of steel and polymer fiber reinforced concrete," *Journal of the Mechanical Behavior of Materials*, vol. 28, no. 1, pp. 119–134, 2019.

[14] B. Arisoy and H. C. Wu, "Material characteristics of high performance lightweight concrete reinforced with PVA," *Construction and Building Materials*, vol. 22, no. 4, pp. 635–645, 2008.

[15] E. A. Flores-Johnson and Q. M. Li, "Structural behaviour of composite sandwich panels with plain and fibre-reinforced foamed concrete cores and corrugated steel faces," *Composite Structures*, vol. 94, no. 5, pp. 1555–1563, 2012.

[16] V. Guerini, A. Conforti, G. Plizzari, and S. Kawashima, "Influence of steel and macro-synthetic fibres on concrete properties," *Fibres*, vol. 6, no. 3, pp. 1–14, 2018.

[17] Y. Wu, W. Song, W. Zhao, and X. Tan, "An experimental study on dynamic mechanical properties of fibre-reinforced concrete under different strain rates," *Applied Sciences*, vol. 8, pp. 1904–10, 2018.

[18] D. Falliano, D. De Domenico, G. Ricciardi, and E. Gugliandolo, "Compressive and flexural strength of fiber-reinforced foamed concrete: effect of fiber content, curing conditions and dry density," *Construction and Building Materials*, vol. 198, pp. 479–493, 2019.

[19] Y. Xu, J. W. Bu, Y. X. Liu, and Y. C. Xu, "Fracture behaviors of rubber concrete under cyclic loading," *Journal of Civil & Environmental Engineering*, vol. 44, no. 1, pp. 142–148, 2020.

[20] R. Ranade, V. C. Li, M. D. Stults, T. S. Rushing, J. Roth, and W. F. Heard, "Micromechanics of high-strength, high-ductility concrete," *ACI Materials Journal*, vol. 110, no. 4, p. 375, 2013.

[21] L. M. Chiacchiarelli, P. Cerrutti, and E. A. Flores-Johnson, "Compressive behavior of rigid polyurethane foams nanostructured with bacterial nanocellulose at low and intermediate strain rates," *Journal of Applied Polymer Science*, vol. 137, no. 20, Article ID 48701, 2020.

[22] M. Frydrych, S. Hysek, L. Fridrichova et al., "Impact of flax and basalt fibre reinforcement on selected properties of geopolymer composites," *Sustainability*, vol. 12, no. 1, p. 118, 2019.

[23] A. Kandemir, T. R. Pozegic, I. Hamerton, S. J. Eichhorn, and M. L. Longana, "Characterisation of natural fibres for sustainable discontinuous fibre composite materials," *Materials*, vol. 13, no. 9, p. 2129, 2020.

[24] FORTA, "FORTA Concrete Fibre," 2021, http://www.Forta-ferro.com/products/Forta-ferro/.

[25] F. Hasan-Nattaj and M. Nematzadeh, "The effect of forta-ferro and steel fibers on mechanical properties of high-strength concrete with and without silica fume and nano-silica," *Construction and Building Materials*, vol. 137, pp. 557–572, 2017.

[26] Y. Liu, Z. Wang, Z. Fan, and J. Gu, "Study on properties of sisal fibre modified foamed concrete IOP Conference Series: materials Science and Engineering," *IOP Conference Series: Materials Science and Engineering*, vol. 744, no. 1, Article ID 012042, 2020.

[27] A. Gautam and A. Awasthi, "Use of FORTA-FERRO fibre in structural concrete mix: a review," *International Research Journal of Engineering and Technology (IRJET)*, vol. 5, no. 5, 2018.

[28] W. Alnahhal and O. Aljidda, "Flexural behavior of basalt fiber reinforced concrete beams with recycled concrete coarse aggregates," *Construction and Building Materials*, vol. 169, pp. 165–178, 2018.

[29] D. Shen, Z. Feng, J. Kang, C. Wen, and H. Shi, "Effect of Barchip fibre on stress relaxation and cracking potential of concrete internally cured with super absorbent polymers," *Construction and Building Materials*, vol. 249, Article ID 118392, 2020.

[30] D. Shen, C. Wen, J. Kang, H. Shi, and Z. Xu, "Early-age stress relaxation and cracking potential of High-strength concrete reinforced with Barchip fiber," *Construction and Building Materials*, vol. 258, Article ID 119538, 2020.

[31] E. A. Alwesabi, B. H. Abu Bakar, I. M. H. Alshaikh, and H. M. Akil, "Impact resistance of plain and rubberized concrete containing steel and polypropylene hybrid fiber," *Materials Today Communications*, vol. 25, Article ID 101640, 2020.

[32] A. Lapko and M. Urbański, "Experimental and theoretical analysis of deflections of concrete beams reinforced with Basalt rebar," *Archives of Civil and Mechanical Engineering*, vol. 15, no. 1, pp. 223–230, Jan. 2015.

[33] Q. Fu, W. Xu, D. Huang et al., "Dynamic non-linear Mohr–Coulomb strength criterion for hybrid Basalt–polypropylene fibre-reinforced concrete under impact loading," *Archives of Civil and Mechanical Engineering*, vol. 21, no. 3, p. 93, 2021.

[34] H. H. Zou, C. M. Song, M. Y. Wang, D. R. Wang, and D. S. Wen, "Experimental and numerical simulation study on the antipenetration properties of fiber ceramic-reactive powder concrete composite targets," *Shock and Vibration*, vol. 2019, Article ID 7673437, 16 pages, 2019.

[35] J. Branston, S. Das, S. Y. Kenno, and C. Taylor, "Mechanical behaviour of Basalt fibre reinforced concrete," *Construction and Building Materials*, vol. 124, pp. 878–886, 2016.

[36] A. Adesina, "Performance of cementitious composites reinforced with chopped Basalt fibres – an overview," *Construction and Building Materials*, vol. 266, Article ID 120970, 2021.

[37] Z. Çelik and A. F. Bingöl, "Fracture properties and impact resistance of self-compacting fiber reinforced concrete (SCFRC)," *Materials and Structures*, vol. 53, no. 3, p. 50, 2020.

[38] G. Y. Cui, X. L. Wang, and D. Y. Wang, "Study on the model test of the antibreaking effect of fiber reinforced concrete lining in tunnel," *Shock and Vibration*, vol. 2020, Article ID 5419650, 11 pages, 2020.

[39] M. Mirdarsoltany, A. Rahai, and F. Hatami, "Experimental investigation on the ductility of concrete deep beams reinforced with basalt-carbon and basalt-steel wire hybrid composite bars," *Shock and Vibration*, vol. 2021, Article ID 6866993, 8 pages, 2021.

[40] H. Taghipoor and A. Sadeghian, "Experimental investigation of single and hybrid-fiber reinforced concrete under drop weight test," *Structures*, vol. 43, pp. 1073–1083, 2022.

[41] A. Amini, A. Abdollahi, M. A. Hariri-Ardebili, and U. Lall, "Copula-based reliability and sensitivity analysis of aging dams: adaptive Kriging and polynomial chaos Kriging methods," *Applied Soft Computing*, vol. 109, Article ID 107524, 2021.

[42] A. Abdollahi, A. Amini, and M. A. Hariri-Ardebili, "An uncertainty-aware dynamic shape optimization framework: gravity dam design," *Reliability Engineering & System Safety*, vol. 222, Article ID 108402, 2022.